Consistent Description of the Metallic Phase of Overdoped Cuprate Superconductors as an Anisotropic Marginal Fermi Liquid

J. Kokalj* and Ross H. McKenzie

School of Mathematics and Physics, University of Queensland, Brisbane, 4072 Queensland, Australia

(Received 22 May 2011; published 26 September 2011)

We consider a model self-energy consisting of an isotropic Fermi liquid term and a marginal Fermi liquid term which is anisotropic over the Fermi surface, vanishing in the same directions as the superconducting gap and the pseudogap. This model self-energy gives a consistent description of experimental results from angle-dependent magnetoresistance, specific heat, de Haas–van Alphen, and measurements of the quasiparticle dispersion near the Fermi surface from photoemission. In particular, we reconcile the strongly doping-dependent anomalous scattering rate observed in angle-dependent magnetoresistance with the almost doping-independent specific heat.

DOI: 10.1103/PhysRevLett.107.147001 PACS numbers: 74.72.Gh, 74.20.Mn, 74.62.−c, 75.47.−m

A key to understanding high-T_c superconductivity may be the anomalous properties of the metallic phase, which are quite distinct from those found in conventional Fermi liquids such as elemental metals. Many properties, such as the pseudogap, are strongly dependent on doping and on the position on the Fermi surface. One can attempt to describe the crucial effect of the strong electron-electron interactions by a frequency- and momentum-dependent electronic self-energy. Angle-resolved photoemission spectroscopy (ARPES) [1] has been used to deduce various forms for the self-energy [2–5] including that of the marginal Fermi liquid phenomenology [6]. However, this approach implicitly assumes the existence of quasiparticles and the associated analytic structure of the one-electron Green's function, which Anderson has contested and proposed an alternative ''hidden Fermi'' liquid (HFL) theory [7].

In this Letter, we consider a model self-energy motivated by angle-dependent magnetoresistance (ADMR) experiments [8–10] and consisting of two terms with distinctly different dependencies on frequency, momentum, and temperature. The first term is that of a Fermi liquid (FL) and is isotropic on the Fermi surface. The second term, which we denote as an anisotropic marginal Fermi liquid (AMFL), has the same frequency and temperature dependence as that of a marginal Fermi liquid, is anisotropic over the Fermi surface, and vanishes in the same directions as the superconducting gap and the pseudogap observed in underdoped cuprates. We present a parametrization of this model self-energy which gives a consistent quantitative description of a wide range of experimental results on overdoped Tl2201 materials, including ADMR, specific heat [11], de Haas–van Alphen [12,13], and the quasiparticle dispersion near the Fermi surface measured by ARPES [14,15]. In particular, we give a consistent description of the strongly doping-dependent anisotropic scattering [9] and the almost doping-independent specific heat [11]. This is possible because, although the scattering can be dominated by the AMFL term, the quasiparticle renormalization is dominated by the FL term. We compare our parametrization of the self-energy with the results of different microscopic theories [16–19] based on Hubbard and t-J models. In particular, we show that predictions of hidden Fermi liquid theory for the temperature and doping dependence of the scattering rate and the magnitude of the specific heat [17,20] are inconsistent with experiment.

Is there a consistent phenomenology of the experiments?—For overdoped materials ADMR provides a complementary probe to ARPES, measuring the Fermi surface (FS) and the quasiparticle (QP) lifetime [8–10] at different points of the FS. Two scattering channels are observed; one has a quadratic temperature (T) dependence and is approximately constant with doping, while the second is approximately linear in T, is anisotropic over the FS [8], and strongly increases with decreasing doping, as optimal doping ($p \simeq 0.16$) is approached from the overdoped regime (see Fig. 1) [9,10]. Information on the self-energy is also provided through the renormalization of quasiparticle energies suggested by specific heat C_V measurements [11], ARPES determination of the Fermi velocity [21], de Haas–van Alphen (dHvA) measurements of the renormalized cyclotron mass [12,13], and the optical effective mass determined from the Drude weight in the frequency-dependent conductivity [22]. All of these suggest a weak doping dependence of the real part of the self-energy, in contrast to the strongly increasing anisotropic scattering rate γ_{aniso} with decreasing doping shown in Fig. 1. This raises a question about consistency because the quasiparticle renormalization and scattering rate are not independent of one another, being related to the real and imaginary parts of the self-energy, respectively. The two parts are related via the Kramers-Kronig relation. Indeed, this relationship is the origin of the unified picture of the Kadowaki-Woods ratio in Fermi liquids [23].

Model self-energy.—Following the temperature dependence and anisotropy of the scattering rate determined by

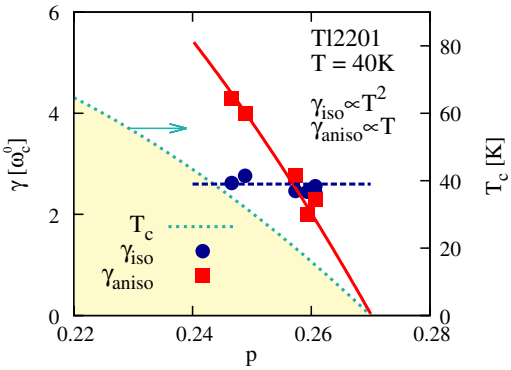

FIG. 1 (color online). Strong doping dependence of the normal state anisotropic scattering rate in an overdoped cuprate superconductor. The scattering rate and its anisotropy are those deduced from the ADMR for Tl2201 at 40 K [9]. The isotropic scattering rate γ_{iso} (points and dashed line), which is constant on the Fermi surface, shows negligible doping dependence. In contrast, the anisotropic scattering rate γ_{aniso} (squares and full line), which is maximal in the antinodal direction and zero in the nodal direction, depends strongly on doping. The doping dependence of γ_{aniso} follows the superconducting transition temperature T_c (dotted line) in this overdoped regime [9,10]. The scattering rates are shown in units of $\omega_c^0 \simeq 1$ meV, the cyclotron frequency at the magnetic field at which the measurements were made.

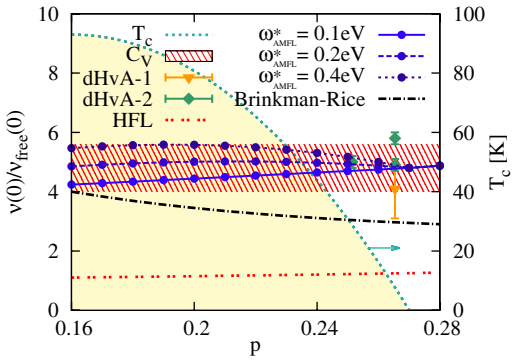

FIG. 2 (color online). Renormalized density of states $\nu(0)/\nu_{free}(0)$ as a function of doping for the anisotropic marginal Fermi liquid model with various values of the cutoff frequency ω^*_{AMFL}. The shaded area shows the range of measured values from C_V [11]. Triangles (dHvA-1) and diamonds (dHvA-2) with error bars show the effective masses deduced from the de Haas–van Alphen effect in Refs. [12,13], respectively. Points with different lines show our estimate deduced from the observed ADMR scattering rate (see Fig. 1) together with Eq. (2) for various ω^*_{AMFL}, $T = 120$ K, and $\omega^*_{FL} = 0.23$ eV. Our estimates are within the measured uncertainties of C_V, which shows that strongly doping-dependent ADMR scattering rates and doping-independent C_V can be consistently described. The Brinkman and Rice result [28] is shown with a dash-dotted line, and the HFL result [20] is shown with a double-dotted line. The density of states is normalized to that for free electrons in two dimensions: $\nu_{free}(0) = 4\pi m_e$.

ADMR, we consider a self-energy consisting of FL and AMFL contributions:

$$\Sigma(\mathbf{k}, \omega) = \Sigma_{FL}(\omega) + \Sigma_{AMFL}(\mathbf{k}, \omega). \quad (1)$$

The detailed functional form is given in the Supplemental Materials. As suggested by the isotropic and $\propto T^2$ scattering rate in ADMR [8,9], we take the FL self-energy isotropic. The AMFL part of the self-energy depends on ϕ [4] (azimuthal angle of the Fermi wave vector $\mathbf{k}_F$ on a 2D FS), and we assume that it is responsible for the anisotropic and T-linear part of the scattering deduced from ADMR [8].

Renormalization of the bare-band mass m_b is determined by $1 - \partial\Sigma'(\phi, \omega)/\partial\omega|_{\omega=0}$, which for our model self-energy gives [24]

$$\frac{m^*(\phi)}{m_b} = Z(\phi)^{-1} = 1 + \frac{4}{\pi}\frac{s}{\omega^*_{FL}} + \lambda(\phi)\ln\left(\frac{\omega^*_{AMFL}}{\pi T}\right), \quad (2)$$

where $Z(\phi)$ is the QP weight at angle ϕ. s parametrizes the strength of the electron-electron scattering associated with the FL term, ω^*_{FL} is the FL high frequency cutoff, $\lambda(\phi)$ is a ϕ-dependent dimensionless AMFL coupling constant, and ω^*_{AMFL} is the AMFL high frequency cutoff. We use units $\hbar = k_B = 1$. In general, there is also a contribution to the renormalization from $\partial\Sigma/\partial k_\perp$, where $k_\perp$ is a momentum perpendicular to the FS. We assume this contribution is negligible [24].

Parametrization of model self-energy.—In the Supplemental Materials, we estimate the parameters in Eq. (2) from the ADMR results and show that $s/\omega^*_{FL} > \lambda(\phi)$ and that $\lambda(\phi)$ vanishes in the nodal direction. Together, this leads to a relatively small effect of the AMFL part of the self-energy on the mass renormalization. Briefly, the isotropic T^2 term gives $s/\omega^{*2}_{FL} \simeq 9.2\ (\text{eV})^{-1}$. The term linear in T gives the strength of the AMFL self-energy and its ϕ dependence [9],

$$\lambda(\phi) = 1.6\cos^2(2\phi)T_c(p)/T_c^{max}, \quad (3)$$

where the doping dependence is encoded via the relation between T_c and p [24]. This expression for $\lambda(\phi)$ explicitly takes into account that the AMFL self-energy is largest in the antinodal direction and zero in the nodal direction [8,10] and that it scales with T_c in the highly overdoped regime [9]. The Fermi liquid cutoff $\omega^*_{FL} \simeq 0.23$ eV is estimated from measurements of C_V in the strongly overdoped regime with $T_c = 0$ which give $m^*/m_e = 4.8 \pm 0.8$ [11]. Estimating the AMFL cutoff ω^*_{AMFL} is discussed below.

Renormalization factor.—Figure 2 shows the calculated density of states at the Fermi energy $\nu(0)$ as a function of doping for various ω^*_{AMFL} together with values deduced from specific heat and de Haas–van Alphen experiments. For the calculation of $\nu(0)$, one evaluates the band mass m_b (or strictly the band density of states at the Fermi energy) from the bare-band dispersion $\epsilon^0_{\mathbf{k}}$, which is approximated with a tight-binding model fit to the LDA bands [Eq. (S7) in the Supplemental Materials [24]]. It is evident from

Fig. 2 that, although the scattering rate of QP in the antinodal direction (or AMFL part of self-energy) strongly increases with decreasing doping, the density of states (and C_V) stays rather constant and is only mildly affected by the AMFL self-energy for all $\omega^*_{\mathrm{AMFL}} \lesssim 0.4$ eV. This is because $m^*/m_b \sim 1 + 4s/\pi\omega^*_{\mathrm{FL}} + \lambda(0)$ for $T \sim 120$ K. Subtleties associated with the relationship between the effective mass and C_V for the AMFL are discussed in the Supplemental Materials [24].

Hence, it is possible for the model self-energy to give a consistent description of the complete doping and temperature dependence of both ADMR [8–10] and C_V measurements [11] with $\omega^*_{\mathrm{FL}} \simeq 0.23$ eV. The results are within measured uncertainty for any $\omega^*_{\mathrm{AMFL}} \lesssim 0.5$ eV which is comparable to previous estimates from ARPES, ~0.2 eV–0.4 eV [4], ~0.1 eV [3], and ~0.4 eV–0.5 eV within the isotropic MFL phenomenology [5,25]. From the above analysis it is evident that not only small ω properties are relevant but also the high-energy cutoffs. These may be reflected as kinks or waterfalls in the QP dispersion [5,26,27].

Renormalized QP dispersion.—Our renormalized dispersion is also in good agreement with the ARPES QP dispersion [14,15] near $(\pi, 0)$ [see Fig. 3(a)], if a small correction of fixing the noninteracting FS to the one measured in ARPES [14] is taken into account by applying a bare-band shift of $[0.17\cos(4\phi) - 0.1\cos(8\phi)]$ eV. The agreement in the nodal direction near the FS is satisfactory, but near the $(0, 0)$ point we observe the waterfall due to the sharp cutoff at ω^*_{FL} [Fig. 3(b)]. The waterfall arises due to $\partial\Sigma'/\partial\omega$ becoming $\gtrsim 1$ in the vicinity of a high frequency cutoff ω^*_{FL} (for example, see Fig. 1 in Ref. [5]). This results in a sharp drop of the QP dispersion and in a broader spectra at $\omega \sim \omega^*_{\mathrm{FL}}$. The discrepancy at the band bottom

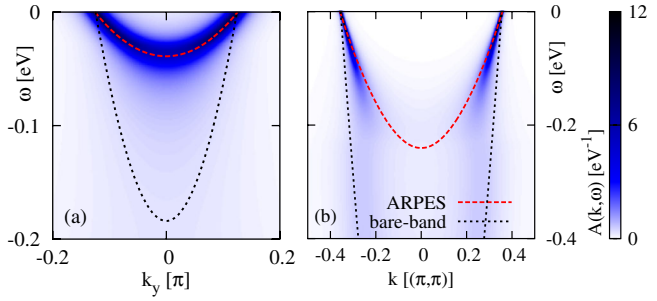

FIG. 3 (color online). Comparison of AMFL spectral function with the quasiparticle dispersion measured by ARPES. Spectral functions calculated with our self-energy ($T = 10$ K, $T_c = 30$ K, $\omega^*_{\mathrm{AMFL}} = 0.2$ eV, $\omega^*_{\mathrm{FL}} = 0.23$ eV) are shown with density plots near the van Hove singularity for $\mathbf{k} = (\pi, k_y)$ (a) and near the band bottom in the nodal direction for $\mathbf{k} = (k, k)$ (b). The agreement with the measured ARPES QP dispersion [14] (dashed line) is very good near the van Hove singularity and at the FS in the nodal direction (b). Some discrepancy is found at the band bottom, where we observe a waterfall originating from ω^*_{FL}. The bare-band dispersion is shown with the dotted line.

may come from difficulties of determining the dispersion from a very broad ARPES spectra or may be an artifact of our approximation for self-energy [24].

Our estimate of λ for the overdoped regime is in satisfactory agreement with the values estimated from ARPES, although some differences are still present [24]. The ARPES estimate for the QP lifetime on the FS [14] in Tl2201 is an order of magnitude larger than that from ADMR and has the opposite angular dependence. This would imply that the renormalization of the effective mass and C_V would be 1 order of magnitude larger, unless the scattering is elastic or some other effects, e.g., surface reconstruction, additionally broaden the ARPES spectra.

To partially conclude, our model self-energy is capable of describing a range of experimental results, including the strongly doping-dependent ADMR scattering rate and almost doping-independent C_V. Earlier, it has been shown that the scattering rate deduced from ADMR can describe the temperature dependence of the intralayer resistivity and Hall coefficient [8,9]. Future studies should examine whether for overdoped cuprates this model self-energy can describe the optical conductivity, asymmetry of tunneling spectra, and ARPES energy distribution curves, particularly since these have been invoked as evidence for the hidden Fermi liquid theory [7].

Microscopic theories.—It is a challenge for microscopic theory to explain large renormalizations of about 4 (see Fig. 3) and the ϕ, T, and p dependence of the self-energy in the overdoped region. The Brinkman-Rice theory [28] predicts too small of a renormalization of $(1 + p)/(2p)$ (Fig. 2), which becomes even smaller if the antiferromagnetic interaction J is taken into account [24]. Within the weak coupling Hubbard model, the MFL component arises from nesting of the Fermi surface or proximity to a van Hove singularity [29,30], but the latter is not applicable to Tl2201 [24]. Functional renormalization group treatment of the Hubbard model shows scattering rates in qualitative agreement with ADMR [16] but predicts an order of magnitude smaller anisotropic scattering rate than observed in experiment [24]. We give a more detailed comparison with microscopic theories in the Supplemental Materials [24] together with candidates of microscopic model calculations, which give a scattering rate similar to our model and of which some may be improved or ruled out if quantitatively compared with our self-energy.

HFL theory.—Anderson has argued that the overdoped cuprates can be described in terms of a Gutzwiller projected Fermi liquid which exhibits power law singularities related to the x-ray edge problem [7]. Casey and Anderson calculated the scattering rate [see Eq. (S10) in the Supplemental Materials [24]] and compared it to ADMR data [17]. However, the scattering rate in HFL [17] has a linear T dependence only for $T \gtrsim W_{\mathrm{HFL}}/2 \sim 400$ K [24], in strong contrast to the ADMR measurements [8], where the T linear term is observed even for $T < 60$ K

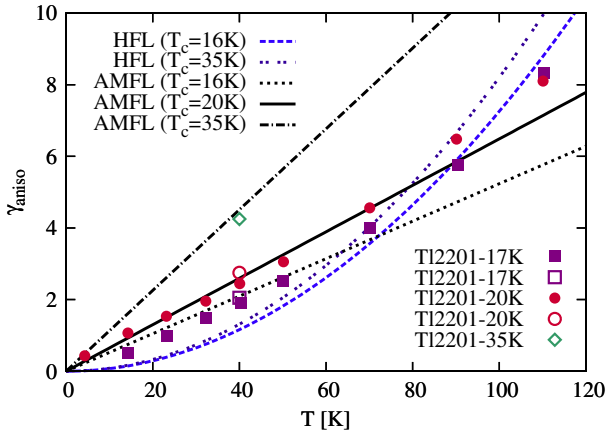

FIG. 4 (color online). HFL theory cannot describe the temperature and doping dependence of the anisotropic scattering, γ_{aniso}. HFL predictions [17] for γ_{aniso} are compared with values deduced from ADMR data [9,10] and to our AMFL parametrization of the ADMR results. HFL predictions [17] for dopings corresponding to $T_c = 16$ and 35 K are shown with dashed and double-dotted lines, respectively. HFL theory does not show any significant linear T dependence at low temperatures, unlike the measured data. (Full symbols are taken from Ref. [10]; empty symbols are from Ref. [9].) Furthermore, HFL shows negligible doping dependence, unlike the significant doping dependence seen in the experimental data. Our AMFL parametrization of the data is shown with dotted, full, and dash-dotted lines. HFL results are obtained with $v_F(0)/v_F(\pi/4) = 0.5$ (as in Ref. [17]), which is kept constant with p.

(see Fig. 4 and Fig. S1 in the Supplemental Materials [24]). W_{HFL} is a HFL bandwidth [24]. Furthermore, they argue that the anisotropic scattering rate deduced from ADMR emerges solely as a consequence of anisotropy of the Fermi momentum and of the Fermi velocity on the FS [17,20]. To obtain anisotropies comparable to ADMR, Casey and Anderson require that $v_F(0)/v_F(\pi/4) \simeq 0.5$. We note that the anisotropy in $v_F(\phi)$ found in LDA calculations is smaller [$v_F(0)/v_F(\pi/4) \simeq 0.8$ [14,31]]. In addition, the LDA calculations show that this ratio increases with increasing doping due to approaching the van Hove singularity [31]. Hence, HFL theory predicts a small increase in the ratio of anisotropic to isotropic scattering with increasing doping (this effect is not taken into account in Fig. 4); the opposite trend is observed with ADMR [9] (see Figs. 4 and S2). Furthermore, HFL predicts $C_V \propto T/\epsilon_F^0$ with no renormalization effects [20], which is significantly smaller than experimental results for Tl2201 (see Fig. 2) [32].

In conclusion, we have shown that it is possible to give a consistent description of a wide range of experimental results for overdoped cuprates in terms of a model self-energy which contains an isotropic Fermi liquid contribution and an anisotropic marginal Fermi liquid contribution. The former is doping-independent, and the latter increases significantly with decreasing doping. This model self-energy is quantitatively inconsistent with some microscopic model calculations and provides an explicit form against which other calculations can be compared. The two distinct terms in the self-energy may have two distinct physical origins. The isotropic Fermi liquid terms arises largely from local physics. The large on site Coulomb repulsion U reduces intersite hopping and leads to Fermi liquid scattering of quasiparticles. Qualitatively, this can be captured in a Brinkman-Rice picture and by dynamical mean-field theory. In contrast, the anisotropic marginal Fermi liquid term arises from nonlocal physics, and its physical origin is unclear. The relative importance of different types of fluctuations (antiferromagnetic, superconducting, or d-density wave), Fermi surface nesting, and proximity to a quantum critical point is unclear.

This work shows that the overdoped cuprates are not simple Fermi liquids as has often been claimed. Instead, they exhibit remnants of some of the same physics present in the optimally doped materials (marginal Fermi liquid behavior) and the underdoped materials (cold spots and well-defined quasiparticles at the same Fermi surface points as the nodes in the superconducting gap and pseudogap). Thus, it seems that the challenge of finding a successful microscopic theoretical description of the metallic phase of the cuprates is now extended to the overdoped regime.

This work was stimulated by discussions with N. E. Hussey. We also acknowledge discussions with A. Carrington, M. Kennett, and B. J. Powell. We thank P. W. Anderson, A. Jacko, and Y. Zhang for comments on the manuscript. Financial support was received from an Australian Research Council Discovery Project grant (No. DP1094395).

*On leave from J. Stefan Institute, Ljubljana, Slovenia.
j.kokalj@uq.edu.au

[1] A. Damascelli, Z. Hussain, and Z. X. Shen, Rev. Mod. Phys. **75**, 473 (2003).
[2] T. Valla *et al.*, Science **285**, 2110 (1999).
[3] A. A. Kordyuk *et al.*, Phys. Rev. Lett. **92**, 257006 (2004).
[4] J. Chang *et al.*, Phys. Rev. B **78**, 205103 (2008).
[5] L. Zhu, V. Aji, A. Shekhter, and C. M. Varma, Phys. Rev. Lett. **100**, 057001 (2008).
[6] C. M. Varma, Int. J. Mod. Phys. B **3**, 2083 (1989).
[7] P. W. Anderson, Nature Phys. **2**, 626 (2006).
[8] M. Abdel-Jawad *et al.*, Nature Phys. **2**, 821 (2006).
[9] M. Abdel-Jawad *et al.*, Phys. Rev. Lett. **99**, 107002 (2007).
[10] M. M. J. French *et al.*, New J. Phys. **11**, 055057 (2009).
[11] J. M. Wade *et al.*, J. Supercond. **7**, 261 (1994); J. W. Loram *et al.*, Physica (Amsterdam) **235C–240C**, 134 (1994).
[12] B. Vignolle *et al.*, Nature (London) **455**, 952 (2008).
[13] A. F. Bangura *et al.*, Phys. Rev. B **82**, 140501 (2010).
[14] M. Platé *et al.*, Phys. Rev. Lett. **95**, 077001 (2005).
[15] D. C. Peets *et al.*, New J. Phys. **9**, 28 (2007).
[16] M. Ossadnik, C. Honerkamp, T. M. Rice, and M. Sigrist, Phys. Rev. Lett. **101**, 256405 (2008).

[17] P. A. Casey and P. W. Anderson, Phys. Rev. Lett. **106**, 097002 (2011).
[18] G. Buzon and A. Greco, Phys. Rev. B **82**, 054526 (2010).
[19] L. Dell'Anna and W. Metzner, Phys. Rev. Lett. **98**, 136402 (2007).
[20] P. A. Casey, Ph.D. thesis, Princeton Physics, 2010, p. 79.
[21] X. J. Zhou *et al.*, Nature (London) **423**, 398 (2003).
[22] W. J. Padilla *et al.*, Phys. Rev. B **72**, 060511 (2005).
[23] A. C. Jacko, J. O. Fjaerestad, and B. J. Powell, Nature Phys. **5**, 422 (2009).
[24] See Supplemental Material at http://link.aps.org/supplemental/10.1103/PhysRevLett.107.147001 for more details.
[25] J. M. Bok *et al.*, Phys. Rev. B **81**, 174516 (2010).
[26] K. Byczuk *et al.*, Nature Phys. **3**, 168 (2007).
[27] M. M. Zemljič, P. Prelovšek, and T. Tohyama, Phys. Rev. Lett. **100**, 036402 (2008).
[28] W. F. Brinkman and T. M. Rice, Phys. Rev. B **2**, 4302 (1970).
[29] R. Roldán, M. P. López-Sancho, F. Guinea, and S. W. Tsai, Phys. Rev. B **74**, 235109 (2006).
[30] G. Kastrinakis, Phys. Rev. B **71**, 014520 (2005).
[31] J. G. Analytis *et al.*, Phys. Rev. B **76**, 104523 (2007).
[32] The HFL result corresponds to the bare-band density of states given, e.g., with the LDA in Ref. [15] or in Ref. [33], where slightly larger values are obtained.
[33] P. M. C. Rourke *et al.*, New J. Phys. **12**, 105009 (2010).